nature structural & molecular biology

# Tudor domain ERI-5 tethers an RNA-dependent RNA polymerase to DCR-1 to potentiate endo-RNAi

Caroline Thivierge[1,2,6], Neetha Makil[1,2,6], Mathieu Flamand[1,2], Jessica J Vasale[3], Craig C Mello[3,4], James Wohlschlegel[5], Darryl Conte Jr[3] & Thomas F Duchaine[1,2]

**Endogenous RNA interference (endo-RNAi) pathways use a variety of mechanisms to generate siRNA and to mediate gene silencing. In *Caenorhabditis elegans*, DCR-1 is essential for competing RNAi pathways—the ERI endo-RNAi pathway and the exogenous RNAi pathway—to function. Here, we demonstrate that DCR-1 forms exclusive complexes in each pathway and further define the ERI–DCR-1 complex. We show that the tandem tudor protein ERI-5 potentiates ERI endo-RNAi by tethering an RNA-dependent RNA polymerase (RdRP) module to DCR-1. In the absence of ERI-5, the RdRP module is uncoupled from DCR-1. Notably, EKL-1, an ERI-5 paralog that specifies distinct RdRP modules in Dicer-independent endo-RNAi pathways, partially compensates for the loss of ERI-5 without interacting with DCR-1. Our results implicate tudor proteins in the recruitment of RdRP complexes to specific steps within DCR-1-dependent and DCR-1-independent endo-RNAi pathways.**



RNA interference, discovered as a gene-silencing mechanism triggered by double-stranded RNA (dsRNA), was initially considered to be a form of sequence-based innate immunity. It was later acknowledged that related mechanisms underlie a continuum of endogenous silencing phenomena in a broad range of organisms[1]. In *Caenorhabditis elegans*, exogenous RNAi (exo-RNAi) is triggered by foreign dsRNA, which is recognized by the type III RNase DCR-1 and its cofactors dsRNA-binding domain protein RDE-4 and putative RNA helicase DRH-1 (ref. 2). DCR-1 processes the dsRNA into short-interfering RNAs (siRNAs), which are specifically loaded onto the Argonaute RDE-1 (refs. 3,4) and serve as a guide, directing RDE-1 to a target mRNA through base pair interactions. Recognition of a target by RDE-1 activates an siRNA amplification system that is dependent on the cellular RNA-dependent RNA polymerases RRF-1 and EGO-1 (refs. 4–7). These so-called secondary siRNAs are synthesized *de novo* by RdRPs and selectively loaded onto a family of worm-specific Argonautes (WAGOs)[4], which effect silencing by transcriptional[8] and/or post-transcriptional means[9].

Endogenous RNAi pathways refer to mechanisms whereby siRNAs are derived from, and converge back on, endogenous loci. Endo-RNAi pathways are pervasive and diverse[10], but many of their underlying mechanistic details are unknown. In *C. elegans*, endo-RNAi pathways are required for a variety of cellular processes, including the assembly and/or maintenance of chromosome integrity[11–13], transposon silencing and transcript surveillance[14], and for a gene-specific regulatory mechanism during early larval development[15]. Many of these endo-RNAi pathways appear to function independently of DCR-1 (ref. 14).

The ERI endo-RNAi pathway is a DCR-1-dependent pathway that functions during sperm development as well as during embryogenesis[13,16,17]. In this pathway, DCR-1 is required for the biogenesis of endo-siRNAs called 26G RNAs, which are 26 nucleotides (nt) with a bias for a monophosphorylated 5′ guanosine[18,19]. The 26G RNAs are loaded into specific Argonaute family members—ALG-3 and ALG-4—in developing sperm cells[16] and in ERGO-1 in the early embryo[20], respectively. In the embryo, the ERI endo-RNAi mechanism activates and competes for the same RdRP-dependent siRNA amplification and WAGO system that is required for the exo-RNAi pathway[13,20,21].

The molecular events that initiate ERI endo-RNAi are unknown. Our previous work identified a number of DCR-1–associated proteins that are required for ERI endo-RNAi, including the RdRP RRF-3, the Dicer-related helicase DRH-3, the tandem tudor domain protein ERI-5, the SAP-exonuclease ERI-1b, as well as the newly discovered proteins ERI-3 and ERI-9 (refs. 13,17,21,22). Recent studies have also revealed that ERI endo-RNAi is dependent on the N-terminal helicase domain of DCR-1 (ref. 22).

In this study, we sought to refine the functional architecture of the exo- and endo-RNAi machineries in *C. elegans*. We demonstrate that two separate DCR-1 complexes are assembled to initiate the exo- and the ERI endo-RNAi pathways. We identify two distinct subunits within the ERI complex (ERIC) and show that an RdRP module composed of RRF-3, DRH-3 and ERI-5 is tethered to DCR-1 to potentiate ERI endo-RNAi. In addition to solving the molecular phenotype of *eri-5*, we demonstrate that paralogous but precisely specified RdRP modules govern DCR-1–dependent and DCR-1–independent RNAi pathways.

[1]Department of Biochemistry, McGill University, Montreal, Quebec, Canada. [2]Goodman Cancer Center, McGill University, Montreal, Quebec, Canada. [3]Program in Molecular Medicine, University of Massachusetts Medical School, Worcester, Massachusetts, USA. [4]Howard Hughes Medical Institute, University of Massachusetts Medical School, Worcester, Massachusetts, USA. [5]Department of Biological Chemistry, David Geffen School of Medicine, University of California Los Angeles, Los Angeles, California, USA. [6]These authors contributed equally to this work. Correspondence should be addressed to T.F.D. (thomas.duchaine@mcgill.ca).

Received 25 June; accepted 14 October; published online 18 December 2011; corrected after print 9 January 2012; doi:10.1038/nsmb.2186

## RESULTS

### DCR-1 is in distinct exo- and endo-RNAi complexes

DCR-1 associates with proteins involved in microRNA, exo-RNAi and endo-RNAi pathways[13]. To examine the distribution of DCR-1 complexes in the exo- and endo-RNAi pathways, we used gel filtration chromatography to resolve DCR-1 complexes in an embryo extract (**Fig. 1a**). Western blot analyses revealed that DCR-1 was present in fractions ranging from 600 to 950 kDa in molecular weight that could be separated into two populations. The peak fractions of DCR-1 (600–700 kDa) cofractionated with factors required for exo-RNAi, including the putative RNA helicase DRH-1 and two isoforms of the dsRNA-binding protein RDE-4 (43 and 46 kDa). A second complex population, representing roughly 43% of DCR-1, (750–950 kDa) cofractionated with ERI endo-RNAi proteins[13], including the SAP-domain exonuclease ERI-1b, the tandem tudor domain protein ERI-5, and the RdRP RRF-3. Notably, the vast majority of ERI-5 and RRF-3 were restricted to fractions corresponding to the 750–950 kDa DCR-1–complex population. Finally, the Dicer-related helicase DRH-3 was present in fractions ranging from ~100 kDa to 950 kDa. Despite this broad distribution, DRH-3 was enriched in fractions containing ERI-1b, ERI-5 and RRF-3 (750–950 kDa) but not in the 600–700 kDa fractions, where the major peak of DCR-1 is found. We note in passing that a substantial portion of ERI-1b, RDE-4 and DRH-3 was detected in fractions of low molecular weight (50–400 kDa), and this could reflect monomeric, dimeric or low molecular complexes involving these proteins. These data suggest that DCR-1 is present in distinct complexes required for exo-RNAi (RDE complex) and endo-RNAi (ERI–DCR-1 complex, or ERIC).

Previous work strongly suggested the existence of an RDE complex comprising DCR-1, RDE-4, DRH-1 and the Argonaute RDE-1 (ref. 2). Indeed, in our study, all of these proteins were detected in immunoprecipitates of endogenous DCR-1, RDE-4 and DRH-1 (**Fig. 1b**). Notably, many of these proteins also relied on each other for their accumulation as well as for their interaction with DCR-1 (see **Supplementary Results** for a detailed description). Furthermore, DCR-1 and DRH-1 were detected after sequential immunoprecipitation of RDE-4 and RDE-1 (**Supplementary Fig. 1**). By contrast, components of ERIC, including ERI-5, DRH-3 and ERI-1b, did not coimmunoprecipitate with DRH-1 (**Fig. 1c**), which was restricted to the RDE complex in our gel filtration experiments. Conversely, DRH-1 did not coimmunoprecipitate with ERI-5, which was restricted to ERIC (**Fig. 1d**), whereas DRH-3 was detected in the ERI-5 immunoprecipitates (**Fig. 1d**). Finally, DRH-1 was detected with the highest peptide coverage in DCR-1 multidimensional protein identification technology (MuDPIT)[13,23] analyses or when conducting MuDPIT analysis of a somatically expressed RDE-4::Flag fusion, whereas

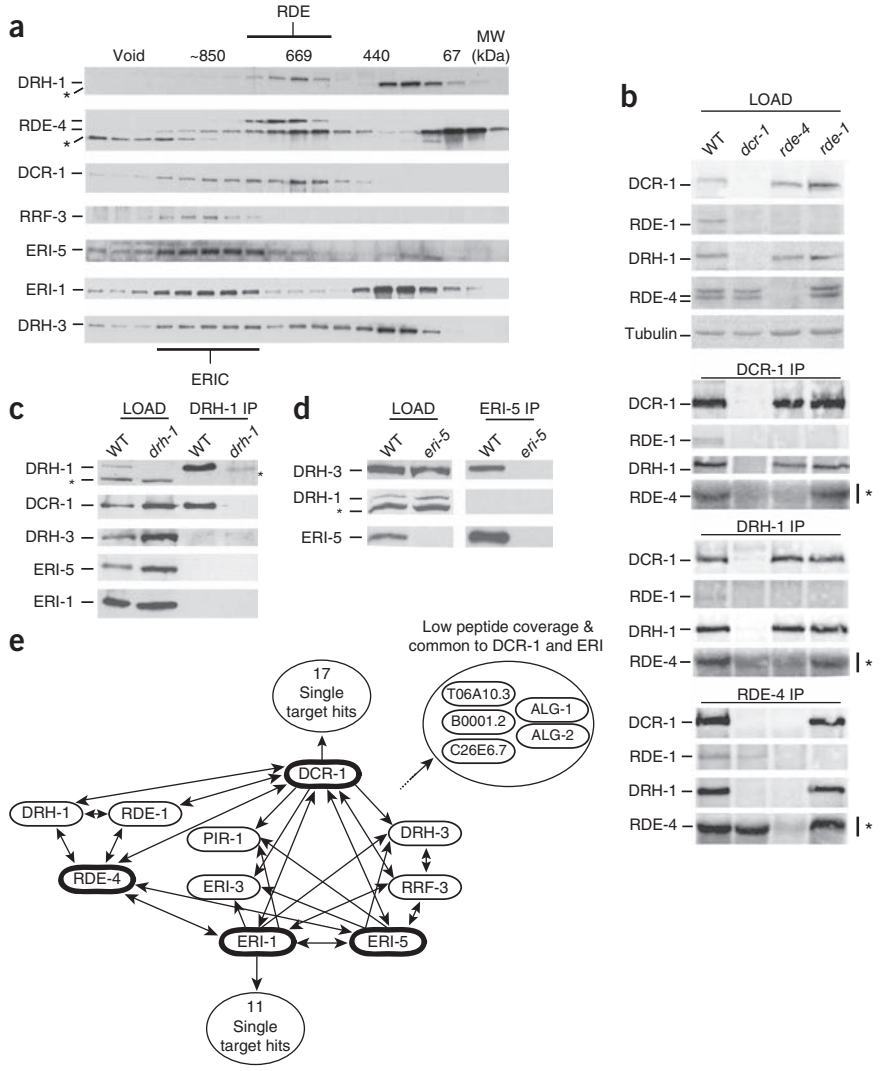


**Figure 1** Distinct DCR-1 complexes initiate endo- and exo-RNAi. (**a**) Gel filtration on wild-type embryonic extract. DRH-1, RDE-4, DCR-1, RRF-3, ERI-5, ERI-1 and DRH-3 proteins were detected by western blot on fractions from a Superose S6 column. The fractionation of molecular weight (MW) standards is indicated. The asterisk (*) labels in DRH-1 (in the low molecular weight fractions) and RDE-4 filtration panels indicate non-specific bands. (**b**) Immunoprecipitation (IP) of DCR-1, DRH-1 and RDE-4 from WT, *dcr-1*, *rde-4* or *rde-1* mutant embryos. DCR-1, RDE-1, DRH-1 and RDE-4 proteins were detected in total lysate (LOAD) and IP by western blot. Tubulin was used as a loading control. The asterisk (*) to the right of the RDE-4 panels indicates background signal from the IgG heavy chains used for immunoprecipitation, which migrate with RDE-4 around 50 kDa. (**c**) Immunoprecipitation of DRH-1 in WT and *drh-1* mutant embryos. DRH-1, DCR-1, DRH-3, ERI-5 and ERI-1 were detected by western blot. The asterisks (*) to the right and left of the DRH-1 panel indicate non-specific bands in the loading and DRH-1 IP lanes, respectively. (**d**) Immunoprecipitation of ERI-5 in WT and *eri-5* mutant embryos. DRH-3, DRH-1 and ERI-5 proteins were detected by western blot. The asterisk (*) indicates the non-specific band detected in the input lanes (LOAD) of the DRH-1 blot, as in panel **c**. (**e**) Interaction map of the proteins detected by MuDPIT analyses in WT embryonic extracts. Proteins circled in bold (DCR-1, ERI-5, ERI-1 and RDE-4) represent immunoprecipitation targets. See Online Methods section for details on the epitope targeted. Arrowheads indicate interactions detected. The interactions of ERI-5 and ERI-1 in RDE-4 immunoprecipitation included in the diagram were only detected by western blotting. The number of interactions detected exclusively in DCR-1 or ERI-1 MuDPIT experiments is indicated (17 or 11 single target hits) and may reflect divergent functions for these proteins.

**Table 1 Comparative proteomics of ERI components**

| Gene | Protein (MW in kDa) | Structural description | No. independent detections (% peptide coverage) ERI-5[a] | ERI-1(Flag)[b] | DCR-1(HA)[b] |
|---|---|---|---|---|---|
| **Common DCR-1, ERI-1 and ERI-5 interactions** | | | | | |
| *Y38F2AR.1* | ERI-5 (61.6) | Tudor domain | 5/5 (19) | 2/2 (9) | 3/3 (24) |
| *F10B5.7* | RRF-3 (201.4) | RdRP | 5/5 (12) | 2/2 (15) | 3/3 (24) |
| *D2005.5* | DRH-3 (129.1) | DEAH/D box RNA helicase. | 4/5 (18) | 2/2 (19) | 3/3 (35) |
| *K12H4.8* | DCR-1 (210.9) | DExH box RNA helicase (Rnase III) | 4/5 (2) | 2/2 (13) | 3/3 (41) |
| *T20G5.11* | RDE-4 (43.4) | dsRBD | 1/5 (6) | 2/2 (11) | 3/3 (44) |
| *W09B6.3* | ERI-3 (66.4) | Novel | 1/5 (4) | 2/2 (12) | 3/3 (33) |
| T07A9.5b | ERI-1b (67.2) | SAP domain, exonuclease | 1/5 (2) | 2/2 (31) | 2/3 (13) |
| *T23G7.5* | PIR-1 (30.1) | RNA phosphatase | 1/5 (7) | 1/2 (8) | 3/3 (47) |
| **Common DCR-1 and ERI-1 Interactions** | | | | | |
| *C26E6.7* | ERI-9 (73.2) | Novel | nd | 2/2 (7) | 3/3 (7) |
| *T06A10.3* | (19.9) | Novel | nd | 2/2 (11) | 2/3 (8) |
| *B0001.2* | (105.1) | Novel | nd | 2/2 (7) | 2/3 (6) |
| *T07D3.7* | ALG-2 (101.6) | Argonaute protein | nd | 2/2 (5) | W[c] |
| *F48F7.1* | ALG-1 (110.9) | Argonaute protein | nd | 2/2 (4) | W[c] |

[a]Immunopurifications of ERI-5 were conducted using a covalently coupled polyclonal matrix. Because peptide coverage varied between independent samples, peptide coverage for the best ERI-5 recovery is used here. [b]Immunoprecipitations conducted on tagged proteins (Flag and HA, as indicated), expressed from null allele-rescuing transgenes[13]. [c]These two proteins were not detected in embryonic DCR-1 proteomic analyses, but they were detected in adult purifications and with embryonic DCR-1 by western blotting (W).



DRH-1 was never detected in ERI-5 or ERI-1 MuDPIT (**Fig. 1e**, below). Taken together, the data indicate that the RDE complex and ERIC are biochemically distinct.

## Comparative proteomics identify ERIC components

We previously reported that the *eri* gene products ERI-1b, ERI-3, ERI-5, RRF-3 and the Dicer-related helicase DRH-3 could be detected in MuDPIT analyses of DCR-1 and ERI-1 (ref. 13). Although both DCR-1 and ERI-1b fractionate in multiple complex populations in gel filtration, the profile of ERI-5 suggests that it is dedicated to ERIC. Therefore, to further define ERIC components, we used MuDPIT to identify proteins that coimmunoprecipitate with ERI-5 and compared these data to previous MuDPIT analyses of DCR-1 and ERI-1 immunoprecipitates[13]. The interactions that could be detected from at least two independent sets of MuDPIT samples and that were never detected in any of the controls are depicted in **Figure 1e** and **Table 1**. DCR-1, ERI-1, ERI-5, ERI-3, DRH-3, RRF-3 and RDE-4 were the only proteins consistently detected for each of the three targets. The PIR-1 putative RNA triphosphatase, previously identified as a DCR-1 interaction[13], was detected in some ERI-5 MuDPIT samples but with a lower peptide coverage. The sum of the masses of these eight proteins (~810 kDa) is generally in accordance with the ~850 kDa mass of ERIC estimated by gel filtration (**Fig. 1a**). This analysis further supports the idea that ERI-5 has only limited or no association outside the ERIC.

Finally, additional proteins were identified in ERI-1 and DCR-1 immunoprecipitates but not in ERI-5 samples (**Fig. 1e** and **Table 1**), including ALG-1, ALG-2, T06A10.3, B0001.2 and ERI-9. These proteins may be transient, indirect or less stable components of ERIC.

## ERI-5 recruits an RdRP module on DCR-1

RRF-3, DRH-3 and DCR-1 were consistently the top ERI-5 interactors, suggesting that ERI-5 is most closely associated with these components of ERIC. This idea is supported by recent work demonstrating that EKL-1, a paralog of ERI-5, interacts with DRH-3 (ref. 14). Notably, the steady-state level of ERI-5 protein was markedly reduced in the *rrf-3(pk1426)* deletion mutant, but it was expressed at wild-type levels in the *rrf-3(mg373)* missense mutant that alters a conserved catalytic residue of RRF-3 (ref. 17) without altering RRF-3 expression (**Fig. 2a**,**b**, top panels, *rrf-3(del)* and *rrf-3(pm)* lanes). Quantitative real-time PCR (qrtPCR) analysis revealed that the *eri-5* mRNA level was unchanged in the *rrf-3(pk1426)* mutant (**Supplementary Fig. 2a**). Together, these results suggest that the stable expression of ERI-5 protein is dependent on RRF-3 protein and indicate a close biochemical relationship between these two proteins. The coupled expression observed for both the RDE complex and ERIC is reminiscent of similar phenomena described in the human Drosha–DGCR8 and fly Dicer2–R2D2 complexes[24,25].

DCR-1, ERI-5, RRF-3 and DRH-3 coimmunoprecipitated with DCR-1 and ERI-5, and these interactions were dependent on ERI-5 and RRF-3 protein (**Fig. 2a**,**b**). For example, RRF-3 and DRH-3 proteins were not detected in DCR-1 immunoprecipitates from *eri-5(tm2528)* or *rrf-3(pk1426)* mutant lysates (**Fig. 2a**, *eri-5* and *rrf-3(del)* lanes). By contrast, the interactions between DCR-1, ERI-5, RRF-3 and DRH-3 remained intact in the *rrf-3(mg373)* catalytic mutant, as well as in *eri-1(mg366)* and *eri-3(tm1361)* mutants (**Fig. 2a**, *rrf-3(pm)*, *eri-1* and *eri-3* lanes). Despite the reduced level of ERI-5 in the *rrf-3(pk1426)* mutant, a substantial amount of ERI-5 was still recovered by ERI-5 immunoprecipitation, but DCR-1 was not detected and DRH-3 was weakly detected. Finally, DCR-1 was not detected in RRF-3 immunoprecipitates in the absence of ERI-5 (see below). Together, these results suggest that ERI-5, RRF-3 and DRH-3 form an interdependent RdRP module and indicate that the tandem tudor domain protein ERI-5 has an important role in the association of this RdRP module to DCR-1. However, these results do not rule out the possibility of additional interactions between RRF-3 and DCR-1 within ERIC. It also indicates that, in stark contrast to its paralog DRH-1, DRH-3 interacts with DCR-1 strictly through RRF-3 and ERI-5.

## ERI proteins interact with the N terminus of DCR-1

Previous work indicated that ERI-3 tethers ERI-1b to DCR-1 (ref. 13). The fact that the interaction between the RdRP module and DCR-1 is independent of *eri-3* and *eri-1* (**Fig. 2a**,**b**) suggests that ERI-5 and ERI-3 recognize distinct sites on DCR-1. To identify the direct binding sites for the ERI machinery on DCR-1, we expressed partially overlapping, recombinant DCR-1 fragments fused to a glutathione *S*-transferase (GST) epitope (**Fig. 2c**, top panel; see

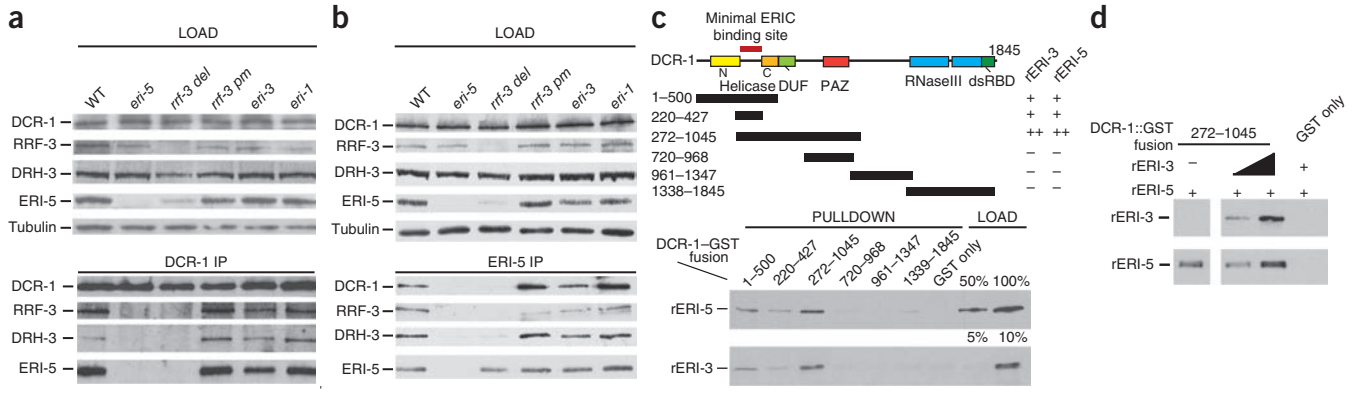


**Figure 2** ERI-5 promotes the association of an RdRP module to the DCR-1 N terminus. (**a**,**b**) Immunoprecipitation (IP) of DCR-1 and ERI-5 in WT, *eri-5*, *rrf-3 del* (deletion mutant, *pk1426*), *rrf-3 pm* (point mutant, *mg373*), *eri-3* and *eri-1* mutant embryos. DCR-1, RRF-3, DRH-3 and ERI-5 were detected by western blotting. Tubulin was used as a loading control. (**c**) Map of the DCR-1–GST constructs used for the GST pulldown of recombinant (r) ERI-5 or ERI-3 (top). The ability of each DCR-1–GST fusion to interact with rERI-5 or rERI-3 was assessed by western blot (bottom panel) to detect recombinant rERI-5-CBP or rERI-3–Flag. The results are summarized to the right of the DCR-1 map; the minus sign denotes weak or no interaction, and the plus sign denotes an interaction (see **Supplementary Fig. 2c** for Coomassie blue gel staining). Percentage (%) of the loading (bottom panel) represents the fraction of rERI-5 and rERI-3 used in the GST pulldown. (**d**) ERI-3 and ERI-5 bind to DCR-1 (272–1045) simultaneously. An increasing amount of rERI-3 was incubated with DCR-1 (272–1045) before addition of rERI-5 and pull-down of the DCR-1 fragment.



**Supplementary Fig. 2b** for Coomassie blue results) and used these DCR-1 fragments as bait to capture recombinant ERI-3 (rERI-3) or ERI-5 (rERI-5) proteins. rERI-5 was pulled down with fragments spanning DCR-1 residues 1–500 and 272–1045. No appreciable interaction could be detected with constructs encoding fusions of residues 720–968, 961–1347 or 1338–1845, or with GST alone (**Fig. 2c**, rERI-5 panel). Maximal binding was observed with a DCR-1 fragment that encodes residues 272–1045. A DCR-1 fragment spanning residues 220–427 still interacted with rERI-5, although slightly less efficiently. rERI-3 was captured by the same DCR-1 fragments that interact with rERI-5, but rERI-3 interacted more weakly overall than rERI-5 did (**Fig. 2c**, rERI-3 panel; compare loading). Thus, the minimal fragment of DCR-1 bound by rERI-5 and rERI-3 (residues 220–427) corresponds to the non-conserved linker between the conserved N- and C-terminal portions of the helicase domain (**Fig. 2c**). However, optimal binding may require additional residues or a contribution by surrounding polypeptide sequences for the folding of this region. These two interactions may occur simultaneously within ERIC, as prebinding increasing amounts of rERI-3 did not preclude, but slightly improved, rERI-5 binding to DCR-1 (**Fig. 2d**). Together with the immunoprecipitation data described above (**Fig. 2a**,**b**), these data suggest that the ERI proteins directly interact with different, and possibly neighboring, sites near the N terminus of DCR-1 (**Fig. 2c**).

### ERI-5 potentiates small RNA biogenesis in ERI endo-RNAi

DCR-1, ERI-1, ERI-3, RRF-3 and DRH-3 are absolutely required for the biogenesis of 26G RNAs and the downstream 22G RNAs[13,20–22,26]. Notably, these small RNA species were only partially reduced in *eri-5* point mutants[13]. The *eri-5(tm2528)* deletion allele used in this study is probably a null allele that completely removes the first tudor domain and alters the reading frame of the remaining *eri-5* locus (**Supplementary Fig. 2c**). Northern blot analyses of small RNAs expressed in embryos revealed that siR26-1, an ERI-dependent 26G RNA derived from the *C40A11.10* ERI target, and 22G RNAs from the X-cluster locus, were only partially reduced in *eri-5(tm2528)* mutants (**Fig. 3a**). These small RNAs were not detected in *rrf-3(pk1425)* mutants (**Fig. 3a**). Using qrtPCR to measure the level of these small RNAs, we estimated that the expression of siR26-1 and of the X-cluster 22G RNA in *eri-5(tm2528)* are one-third to one-quarter of the wild-type level (**Fig. 3b**).

The reduced level of the ERI-dependent endo-siRNAs suggested that ERI-5 could have a role in either the specificity or the efficiency of 26G-RNA biogenesis. To measure the overall level of 26G RNAs in the *eri-5* mutant, we cloned and deep-sequenced small RNAs from *eri-5*, *rrf-3* and wild-type embryos using a method that is compatible with small RNAs having a 5′ monophosphate, including 26G RNAs, miRNAs and 21U RNAs[18,19]. As expected, 26G RNAs were completely abolished in *rrf-3* mutant embryos (**Fig. 3c**). Of the few 26-nt sequences cloned from the *rrf-3* sample, most were reads with a 5′ adenine and primarily corresponded to miRNA precursors or to mRNA degradation products. The overall 26G-RNA level was reduced by ~50% in *eri-5* embryos relative to wild-type (**Supplementary Fig. 3a**,**b**), consistent with northern blot and qrtPCR analyses of siR26-1. The 26G RNAs that were cloned from *eri-5* mutant embryos map to the previously defined 26G-RNA loci and are not derived from new loci (**Fig. 3c** and data not shown)[20], indicating that the specificity of ERI endo-RNAi remains unchanged in the *eri-5* mutant. 26G-RNA reads targeting more than 75% of genes and 50% of non-annotated loci were depleted (**Fig. 3c**, left panel). The median levels of 26G RNAs targeting genes and non-annotated loci were four times and two times lower, respectively, in the *eri-5* mutant than in the wild type. Together, these results suggest that ERI-5 promotes the efficiency of 26G-RNA biogenesis by coupling the activities of RRF-3 and DCR-1.

To analyze 22G RNAs in *eri-5(tm2528)*, we cloned small RNAs from adult animals using a method compatible with small RNAs having a 5′ triphosphate[14]. Consistent with the X-cluster northern blot analysis (**Fig. 3a**), 22G RNAs targeting 26G-RNA loci were substantially reduced in the *eri-5* mutant, but less severely than in the *rrf-3* mutant (**Fig. 3c**, right panel). The median depletion of 22G RNAs targeting 26G-RNA loci was by nine times in the *eri-5* mutant and by 50 times in the *rrf-3* mutant (**Fig. 3c**). As previously observed for *ergo-1* and *rrf-3* mutants[20], the ERI-independent 22G-RNA populations that are important for genome surveillance and chromosome segregation appear to be unaffected in the *eri-5* mutant (**Supplementary Fig. 3c**,**d**). These findings suggest that efficient 26G-RNA biogenesis is important for the amplification and accumulation of the downstream 22G RNAs in the ERI pathway.

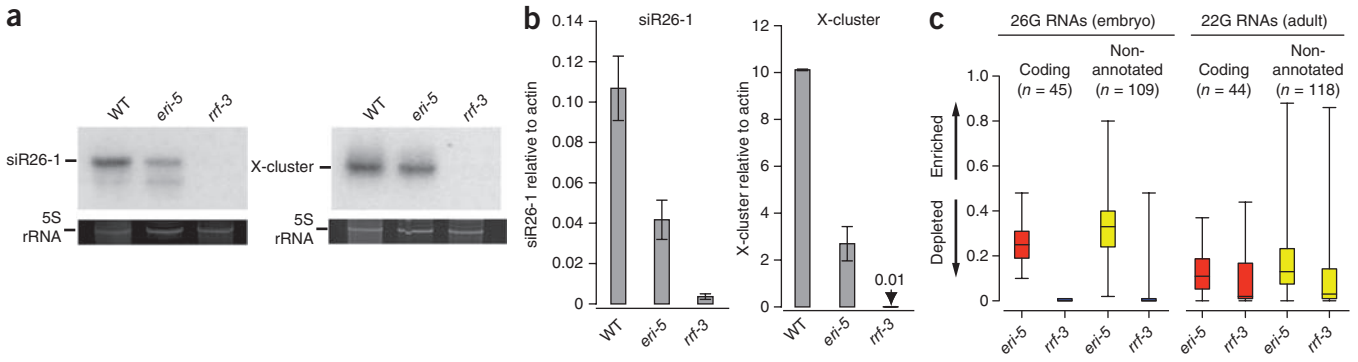


**Figure 3** ERI-5 potentiates ERI endo-RNAi small RNA biogenesis. (**a**,**b**) Northern (**a**) and qrtPCR analysis (**b**) of *C40A11.10* 26G-RNA siRNA species (siR26-1) as indicated in WT, *eri-5* and *rrf-3 (pk1426)* mutant embryos. The *C40A11.10* probe detected both 26G and 22G RNAs. 5S ribosomal RNA (rRNA) ethidium bromide staining is shown as a loading control in **a**. The mean of at least three independent experiments is depicted as the ratio of siR26-1 or X-cluster relative to actin. Error bars indicate s.d. (**c**) Box and whisker plots show the enrichment or depletion of small RNAs targeting 26G-RNA coding genes (red) and non-annotated 26G-RNA clusters (yellow) in the indicated mutant. The left panel is an analysis of 26-nt antisense reads from embryo small RNA libraries that target the 26G-RNA loci. The right panel is an analysis of all antisense reads from adult small RNA libraries that target the 26G-RNA loci. The majority of reads in the adult samples are 22G RNAs. Values approaching 1 indicate enrichment of small RNA; values approaching 0 indicate depletion. Relative enrichment was calculated as the ratio of mutant per (mutant plus wild type). The top and bottom of each box represent the 75th and 25th percentiles, respectively. The horizontal line within each box represents the median value. The number of loci used to generate box and whisker plots is indicated above each plot, and the data are provided in **Supplementary Data 1** and **2**.



## ERI endo-siRNA biogenesis requires tudor domain proteins

Our data indicate that a complete loss of ERI-5, which uncouples the interaction of RRF-3 with DCR-1, results in a reduction of ERI endo-siRNAs. One possible explanation for this partial loss of endo-siRNAs is that EKL-1, a paralog of ERI-5, may partially compensate for the loss of ERI-5. To test this hypothesis, we measured *C40A11.10* 26G-RNA levels by qrtPCR in the *eri-5(tm2528)* animals in which *ekl-1* was depleted by RNAi. Because a strong exo-RNAi response can mildly reduce endo-siRNA levels[13], we used *sel-1*(RNAi) as a negative control (**Fig. 4a**,**b**, **Supplementary Fig. 4**). *ekl-1*(RNAi) alone did not affect the level of *C40A11.10* 26G RNAs, indicating that EKL-1 does not normally contribute to 26G-RNA biogenesis. However, *ekl-1*(RNAi) obliterated the remaining 26G RNAs in the *eri-5(tm2528)* mutant (**Fig. 4a**,**b**), indicating that EKL-1 is not redundant with ERI-5 but can partially compensate for the loss of ERI-5 in the production of at least some of the endo-siRNAs.

Because EKL-1 is required for small RNA pathways that are independent of DCR-1 (refs. 12,14), we addressed the possibility that molecular replacement of ERI-5 by EKL-1 may have altered the requirements for 26G-RNA biogenesis. In particular, we asked whether the 26G RNAs that remain in the *eri-5* mutant are dependent on DCR-1. We took advantage of an Eri allele of *dcr-1*, *eri-4(mg375)*, which carries a missense mutation in the helicase domain of *dcr-1* and completely abrogates ERI-dependent endo-siRNAs, including the 26G RNAs, while maintaining interactions between ERIC components[17,22]. Indeed, *C40A11.10* 26G RNAs were completely dependent on ERI-4. *eri-4(mg375)* completely abolished the EKL-1-dependent 26G RNAs that accumulated in the *eri-5(tm2528)* background (**Fig. 4c**, *eri-5* and *eri-4*). Although the 26G RNAs that accumulated in the absence of ERI-5 were dependent on EKL-1 and DCR-1, a stable interaction between EKL-1 and DCR-1 was not detected in reciprocal immunoprecipitation experiments (**Fig. 4d**). Therefore, although RRF-3 and DCR-1 do not stably interact in the *eri-5* mutant, DCR-1 is nonetheless required for the production of EKL-1-dependent 26G RNAs.

Because EKL-1 partially compensates for the loss of ERI-5, we asked whether EKL-1 coimmunoprecipitates with RRF-3 in WT and

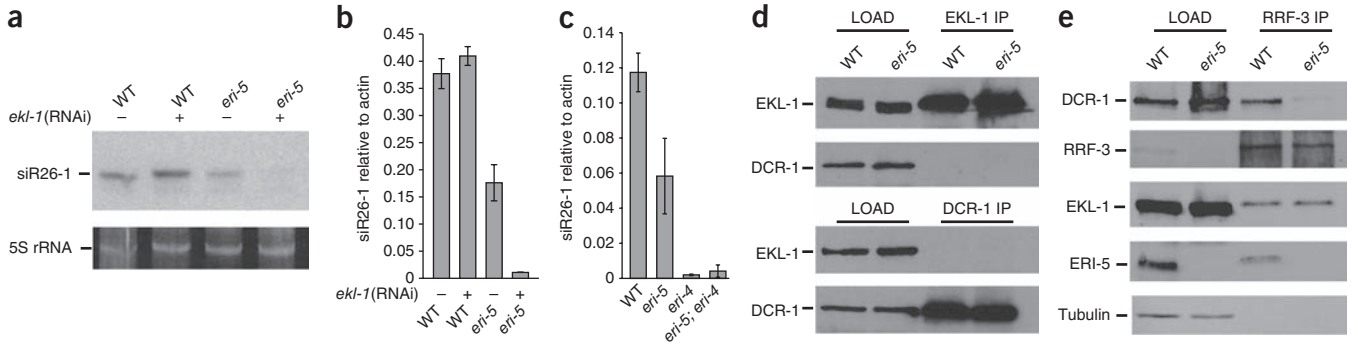


**Figure 4** Tandem tudor domain proteins are required for ERI endo-siRNA biogenesis. (**a**,**b**) Northern (**a**) and qrtPCR (**b**) analysis of *C40A11.10* 26G RNAs (siR26-1) in *sel-1* (RNAi) (a negative control, marked with (–)), *ekl-1*(RNAi), *eri-5* and *eri-5*, and in *ekl-1*(RNAi) embryos. The mean of at least three independent experiments is depicted as the ratio of siR26-1 relative to actin. Error bars indicate s.d. (**c**) qrtPCR analysis of *C40A11.10* 26G RNAs (siR26-1) in WT, *eri-5*, *eri-4* and double *eri-5*, and in *eri-4* mutant embryos. The mean of at least three independent experiments is depicted as the ratio of siR26-1 relative to actin. Error bars indicate s.d. (**d**) IP of EKL-1 and DCR-1 in WT and eri-5 mutant embryos. EKL-1 and DCR-1 proteins were detected by western blot. (**e**) Immunoprecipitation of RRF-3 in WT and *eri-5* mutant embryos. DCR-1, RRF-3, EKL-1 and ERI-5 proteins were detected by western blot. Tubulin was used as a loading control.

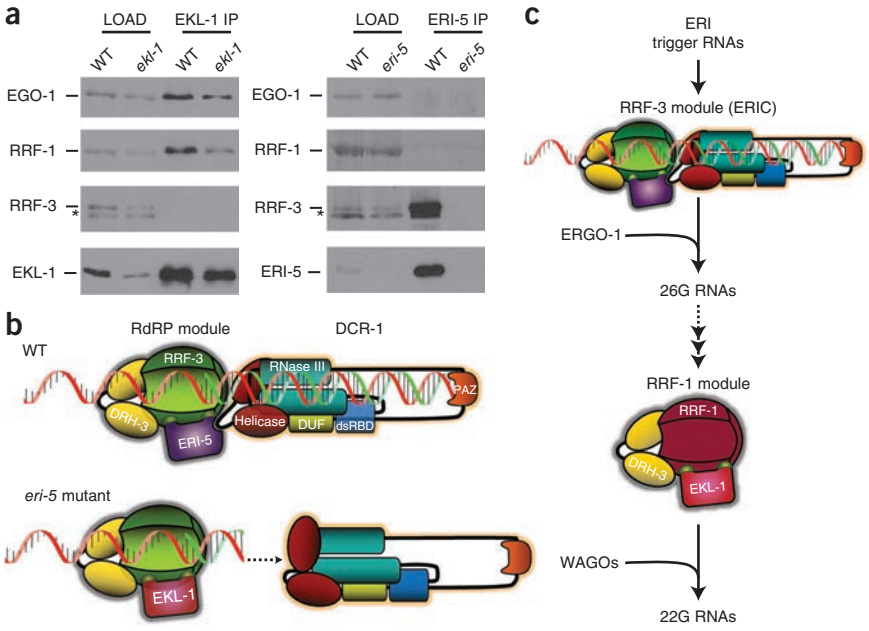


**Figure 5** Roles and paralog organization of RdRP modules in ERI endo-RNAi. (**a**) IP of EKL-1 in WT and *ekl-1*(RNAi) (*ekl-1* lanes) embryos, and immunoprecipitation of ERI-5 in WT and *eri-5* mutant embryos. The RdRPs EGO-1, RRF-1 and RRF-3, and the tudor domain proteins EKL-1 and ERI-5 were detected by western blot. Asterisk (*) indicates a non-specific band. (**b**) Model of the molecular compensation of ERI-5 by EKL-1. Interactions between the RdRP module and the N-terminal helicase domain of DCR-1 couple the generation of dsRNA by RRF-3 with processive DCR-1 activity. In the *eri-5* mutant, this coupling is lost and the autoinhibitory function of the helicase domain predominates, resulting in inefficient 26G-RNA production. (**c**) Paralogous RdRP modules function sequentially in ERI endo-RNAi. An RdRP module comprised of RRF-3, DRH-3 and ERI-5 together with DCR-1 function at the initial step to generate 26G RNAs, the primary siRNAs of the ERI pathway that programs ERGO-1. A paralogous RdRP module comprised of RRF-1, DRH-3 and EKL-1 is responsible for secondary siRNA generation that is independent of DCR-1. This abundant pool of small RNAs programs the WAGO Argonautes to effect endo-RNAi silencing. Paralogous EGO-1 complexes may be involved in this and other RNAi pathways. Some of the ERIC components were omitted from the model for clarity.



*eri-5* backgrounds. To our surprise, a small fraction of EKL-1 copurified with RRF-3 equally well in both WT and *eri-5* backgrounds (**Fig. 4e**). These results indicate that a minor fraction of EKL-1 normally interacts with RRF-3, but its contribution to 26G-RNA biogenesis is only observed in the absence of ERI-5.

### Tandem tudor domain proteins define paralogous RdRP modules

The molecular replacement of ERI-5 by EKL-1 in the RRF-3 RdRP module suggests that the RdRPs RRF-1 and EGO-1 may adopt the same modular organization in the other RNAi pathways. Indeed, other workers[14] recently demonstrated that EKL-1 and the RdRPs RRF-1 and EGO-1 coimmunoprecipitate with DRH-3 and function in multiple DCR-1–independent endo-RNAi pathways. Hence, at least three independent RdRP modules may coexist in *C. elegans* to specifically orchestrate different steps in RNAi pathways. To test this hypothesis, we immunoprecipitated EKL-1 and ERI-5 proteins, and we identified the associated RdRPs by western blot. Both EGO-1 and RRF-1 efficiently coimmunoprecipitated with EKL-1 (**Fig. 5a**, left panel). Although RRF-3 immunoprecipitation revealed a weak interaction with EKL-1 (**Fig. 4e**), RRF-3 was not detected in the EKL-1 immunoprecipitates. Furthermore, although RRF-3 was strongly enriched by ERI-5 immunoprecipitation, EGO-1 or RRF-1 were not detected in the ERI-5 immunoprecipitates (**Fig. 5a**, right panel). Altogether, our results indicate that tandem tudor proteins specify RdRP modules in DCR-1–dependent and DCR-1–independent RNAi pathways (see model in **Fig. 5b**,**c** and Discussion).

## DISCUSSION

Using a combination of molecular and proteomics approaches, we demonstrate that DCR-1 forms distinct complexes that mediate exo-RNAi (RDE complex) and ERI endo-RNAi (ERIC). Our analysis of ERIC indicates that an RdRP module comprised of RRF-3, DRH-3 and ERI-5 is recruited to DCR-1 by the tandem tudor domain protein ERI-5. Furthermore, this report reveals the importance of interactions between RdRPs, tandem tudor domain proteins and DCR-1 and provides a comprehensive interaction framework for the functional organization of RdRPs in *C. elegans*.

### The significance of DCR-1 interaction for ERI endo-RNAi

ERIC is composed of RRF-3, ERI-5 and DRH-3 (an RdRP module), ERI-1 and ERI-3 (together), RDE-4, and additional proteins that possibly interact in a transient or unstable manner. The physical coupling between DCR-1 and an RdRP presented here is reminiscent of the molecular organization of Dicer–RdRP complexes described in *Schizosaccharomyces pombe* and *Tetrahymena thermophila*[27,28]. Notably, in *S. pombe* the C-terminal dsRNA binding domain of Dcr1 both physically and functionally couples the RdRP complex to Dcr1 (ref. 27). By contrast, within ERIC, both the RdRP module and the ERI-1–ERI-3 module bind to the N terminus of DCR-1. The configuration of each complex is essential to promote efficient siRNA synthesis. The interaction between the RdRP module and the N terminus of DCR-1 probably has additional implications, in light of the properties recently attributed to this region. The ATPase activity of the helicase domain of DCR-1 is essential for 26G-RNA accumulation and ERI endo-RNAi[22]. Furthermore, the ATPase activity is required for recognition and processing of blunt-ended dsRNA substrates into 26-nt siRNAs *in vitro*[29]. Notably, the N terminus of human Dicer exerts an autoinhibitory function on its Rnase III activity[30]. How can the known functions of the N terminus of DCR-1 be linked with its scaffolding of the ERI endo-RNAi machinery? The interaction between ERI proteins and the helicase domain of DCR-1 effectively couple the generation of dsRNA by RRF-3 to the processive mode of DCR-1 responsible for 26G-RNA generation[29]. The interactions within ERIC may mediate conformational changes that stimulate DCR-1 activity (**Fig. 5b**, WT panel). In the absence of these interactions (for example, in the *eri-5* mutant), the autoinhibitory function of the helicase domain of DCR-1 predominates, resulting in inefficient 26G-RNA production (**Fig. 5b**, *eri-5* mutant).

Although this is an attractive model, a number of questions on the biogenesis of 26G siRNAs in ERI endo-RNAi remain, including

the asymmetric accumulation of antisense 26G siRNAs and the strong bias for the 5′ guanosine nucleotide. Answers to these lingering conundrums will require further characterization of each module, recapitulation of the ERIC, using recombinant proteins, and additional structural details regarding the dynamic organization of ERIC.

### Functional organization of paralog RdRP modules in RNAi

A number of previous publications have linked EKL-1 and DRH-3 to various endo- and exo-RNAi functions[7,12–15]. Of particular relevance to the present work, one study found that EKL-1 and the RdRPs RRF-1 and EGO-1 were present in DRH-3 immunoprecipitates and postulated that these proteins were assembled as a core complex to mediate RdRP functions in multiple endo-RNAi pathways[14]. The results presented here refine and extend this view. Indeed, our data reveal that RRF-3, EGO-1 and RRF-1 are assembled into analogous modules composed of an RdRP, a tandem tudor domain protein and the DRH-3 helicase. However, these modules participate in markedly different mechanisms of small RNA biogenesis. Whereas the EGO-1 and RRF-1 modules are capable of generating small RNAs in a DCR-1–independent manner[7], the RRF-3 module requires DCR-1 and several other factors, including ERI-1 and ERI-3, for efficient generation of the 26G RNAs. This unusual mechanistic diversification of paralogous RdRP modules is emphasized by sequential activity of distinct RdRP modules in the ERI endo-RNAi pathway (**Fig. 5c**)[20,21]. Thus, our findings indicate that the specificity of paralogous RdRP modules is imparted by the tandem tudor domain proteins ERI-5 and EKL-1.

### The roles of tandem tudor domain proteins in RNAi

Our data indicate that the tandem tudor domain proteins ERI-5 and EKL-1 carry out at least two distinct functions in ERIC. First, they are essential cofactors for RRF-3 activity, and second, the interaction with ERI-5 is essential for the stable recruitment of RRF-3 to DCR-1. Although EKL-1 palliates, at least partially, the 26G-RNA defects in the *eri-5* mutant, it cannot compensate for the defect in DCR-1 recruitment, resulting in attenuated ERI endo-RNAi. The partial molecular compensation by EKL-1 indicates that a stable association with DCR-1 potentiates, but is not essential for, 26G-RNA biogenesis.

In the absence of ERI-5, EKL-1 does not appear to alter the target specificity of ERI endo-RNAi. Furthermore, DRH-3 is a common component of RdRP modules in *C. elegans*. Hence, it is unlikely that DRH-3 or the tandem tudor domain proteins act as determinants that recognize the ERI endo-RNAi triggers. Possible determinants may lie within the N terminus of RRF-3, a portion that has diverged considerably from the other RdRPs in *C. elegans*. Alternatively, additional ERIC components may behave as *trans*-acting factors that recognize the RNA template.

Tudor domains adopt a fold similar to the chromodomains and bind to methylated derivatives of arginine or lysine[31,32]. Our evidence suggests that ERI-5 may recognize such modified amino acids within ERIC. The essential role of ERI-5 in recruiting RRF-3 to DCR-1, the high peptide coverage for RRF-3 in ERI-5 MuDPIT experiments, and the coupled stability of ERI-5 protein with RRF-3 indicate a robust—and probably direct—interaction between ERI-5 and RRF-3. Yet, recombinant RRF-3 (which may not be methylated *in vitro*) did not interact directly with recombinant ERI-5 *in vitro* (data not shown), whereas ERI-5 strongly binds DCR-1 under the same conditions. Therefore, we speculate that *in vivo* modification of RRF-3 (although we do not rule out DRH-3) generates tudor domain–binding sites for ERI-5 and/or EKL-1 (**Fig. 5b**,**c**). In light of the role of EKL-1 in paralogous RdRP modules as well as its compensatory function in *eri-5* mutants, a similar interaction between EKL-1 and the RdRPs RRF-1, EGO-1 or RRF-3 could occur. Hence, the identification of the modified amino acids within RRF-3 and within the other RdRPs represents an important next avenue of research. We note that this hypothesized function of the tandem tudor domains of ERI-5 and EKL-1 is quite distinct from—but not mutually exclusive of—the proposed RITS-like interaction between EKL-1 and chromatin marks in the CSR pathway[12].

## METHODS

Methods and any associated references are available in the online version of the paper at http://www.nature.com/nsmb/.

*Note: Supplementary information is available on the Nature Structural & Molecular Biology website.*


### ACKNOWLEDGMENTS

We thank C. Rocheleau for comments on the manuscript, N. Uetani for conceptual and artistic contributions to the model, S. Mitani and his group at the Department of Physiology, Tokyo Women's Medical University School of Medicine, for the generation of the *eri-5(tm2528)* allele introduced in this manuscript. We thank I. MacRae and N. Welker for discussions on the ERIC model. We also thank A. Haggarty for her assistance in the development of some of the polyclonal antisera. This work was supported by the National Sciences and Engineering Council of Canada RGPIN 341457 (T.F.D.), the Canadian Institute of Health Research MOP 86577 (T.F.D.), the Canada Foundation for Innovation (C.F.I.), and the Fonds de la Rercherche en Santé du Québec, Chercheur-Boursier Salary Award J2 (T.F.D.).


### AUTHOR CONTRIBUTIONS

C.T. conducted the experiments presented in Figures 1c, 2c,d, 3a,b, 4a,b,d and 5a, prepared the figures and assisted with the preparation of the manuscript. N.M. conducted the experiments presented in Figure 1a,d, the ERI-5 samples in 1e and 2a,b. M.F. conducted the experiments presented in Figure 4b,d, and assisted with the model. J.W. carried out the MuDPIT analyses of IP samples. D.C. and J.J.V. conducted the experiments in Figure 3c, under C.C.M.'s direction. D.C. provided scientific advice, and assisted with the redaction of the manuscript. T.F.D. conducted the experiments in Figure 1b, wrote the manuscript and directed the project.

### COMPETING FINANCIAL INTERESTS

The authors declare no competing financial interests.


Published online at http://www.nature.com/nsmb/.
Reprints and permissions information is available online at http://www.nature.com/reprints/index.html.



1. Mello, C.C. & Conte, D. Jr. Revealing the world of RNA interference. *Nature* **431**, 338–342 (2004).
2. Tabara, H., Yigit, E., Siomi, H. & Mello, C.C. The dsRNA binding protein RDE-4 interacts with RDE-1, DCR-1, and a DExH-box helicase to direct RNAi in *C. elegans*. *Cell* **109**, 861–871 (2002).
3. Tabara, H. *et al.* The rde-1 gene, RNA interference, and transposon silencing in *C. elegans*. *Cell* **99**, 123–132 (1999).
4. Yigit, E. *et al.* Analysis of the *C. elegans* Argonaute family reveals that distinct Argonautes act sequentially during RNAi. *Cell* **127**, 747–757 (2006).
5. Pak, J. & Fire, A. Distinct populations of primary and secondary effectors during RNAi in *C. elegans*. *Science* **315**, 241–244 (2007).
6. Sijen, T., Steiner, F.A., Thijssen, K.L. & Plasterk, R.H. Secondary siRNAs result from unprimed RNA synthesis and form a distinct class. *Science* **315**, 244–247 (2007).
7. Aoki, K., Moriguchi, H., Yoshioka, T., Okawa, K. & Tabara, H. *In vitro* analyses of the production and activity of secondary small interfering RNAs in *C. elegans*. *EMBO J.* **26**, 5007–5019 (2007).
8. Guang, S. *et al.* Small regulatory RNAs inhibit RNA polymerase II during the elongation phase of transcription. *Nature* **465**, 1097–1101 (2010).
9. Fire, A. *et al.* Potent and specific genetic interference by double-stranded RNA in *Caenorhabditis elegans*. *Nature* **391**, 806–811 (1998).
10. Ketting, R.F. The many faces of RNAi. *Dev. Cell* **20**, 148–161 (2011).
11. Talsky, K.B. & Collins, K. Initiation by a eukaryotic RNA-dependent RNA polymerase requires looping of the template end and is influenced by the template-tailing activity of an associated uridyltransferase. *J. Biol. Chem.* **285**, 27614–27623 (2010).
12. Claycomb, J.M. *et al.* The Argonaute CSR-1 and its 22G-RNA cofactors are required for holocentric chromosome segregation. *Cell* **139**, 123–134 (2009).

13. Duchaine, T.F. *et al.* Functional proteomics reveals the biochemical niche of *C. elegans* DCR-1 in multiple small-RNA-mediated pathways. *Cell* **124**, 343–354 (2006).
14. Gu, W. *et al.* Distinct argonaute-mediated 22G-RNA pathways direct genome surveillance in the *C. elegans* germline. *Mol. Cell* **36**, 231–244 (2009).
15. Rocheleau, C.E. *et al.* The *Caenorhabditis elegans* ekl (enhancer of ksr-1 lethality) genes include putative components of a germline small RNA pathway. *Genetics* **178**, 1431–1443 (2008).
16. Conine, C.C. *et al.* Argonautes ALG-3 and ALG-4 are required for spermatogenesis-specific 26G-RNAs and thermotolerant sperm in *Caenorhabditis elegans*. *Proc. Natl. Acad. Sci. USA* **107**, 3588–3593 (2010).
17. Pavelec, D.M., Lachowiec, J., Duchaine, T.F., Smith, H.E. & Kennedy, S. Requirement for the ERI/DICER complex in endogenous RNA interference and sperm development in *Caenorhabditis elegans*. *Genetics* **183**, 1283–1295 (2009).
18. Batista, P.J. *et al.* PRG-1 and 21U-RNAs interact to form the piRNA complex required for fertility in *C. elegans*. *Mol. Cell* **31**, 67–78 (2008).
19. Ruby, J.G. *et al.* Large-scale sequencing reveals 21U-RNAs and additional microRNAs and endogenous siRNAs in *C. elegans*. *Cell* **127**, 1193–1207 (2006).
20. Vasale, J.J. *et al.* Sequential rounds of RNA-dependent RNA transcription drive endogenous small-RNA biogenesis in the ERGO-1/Argonaute pathway. *Proc. Natl. Acad. Sci. USA* **107**, 3582–3587 (2010).
21. Gent, J.I. *et al.* Distinct phases of siRNA synthesis in an endogenous RNAi pathway in *C. elegans* soma. *Mol. Cell* **37**, 679–689 (2010).
22. Welker, N.C. *et al.* Dicer's helicase domain is required for accumulation of some, but not all, *C. elegans* endogenous siRNAs. *RNA* **16**, 893–903 (2010).
23. Wolters, D.A., Washburn, M.P. & Yates, J.R. III. An automated multidimensional protein identification technology for shotgun proteomics. *Anal. Chem.* **73**, 5683–5690 (2001).
24. Gu, S.G. *et al.* Distinct ribonucleoprotein reservoirs for microRNA and siRNA populations in *C. elegans*. *RNA* **13**, 1492–1504 (2007).
25. Liu, Q. *et al.* R2D2, a bridge between the initiation and effector steps of the *Drosophila* RNAi pathway. *Science* **301**, 1921–1925 (2003).
26. Han, T. *et al.* 26G endo-siRNAs regulate spermatogenic and zygotic gene expression in *Caenorhabditis elegans*. *Proc. Natl. Acad. Sci. USA* **106**, 18674–18679 (2009).
27. Colmenares, S.U., Buker, S.M., Buhler, M., Dlakic, M. & Moazed, D. Coupling of double-stranded RNA synthesis and siRNA generation in fission yeast RNAi. *Mol. Cell* **27**, 449–461 (2007).
28. Lee, S.R. & Collins, K. Physical and functional coupling of RNA-dependent RNA polymerase and Dicer in the biogenesis of endogenous siRNAs. *Nat. Struct. Mol. Biol.* **14**, 604–610 (2007).
29. Welker, N.C. *et al.* Dicer's helicase domain discriminates dsRNA termini to promote an altered reaction mode. *Mol. Cell* **41**, 589–599 (2011).
30. Ma, E., MacRae, I.J., Kirsch, J.F. & Doudna, J.A. Autoinhibition of human dicer by its internal helicase domain. *J. Mol. Biol.* **380**, 237–243 (2008).
31. Maurer-Stroh, S. *et al.* The Tudor domain 'Royal Family': Tudor, plant Agenet, Chromo, PWWP and MBT domains. *Trends Biochem. Sci.* **28**, 69–74 (2003).
32. Thomson, T. & Lasko, P. *Drosophila* tudor is essential for polar granule assembly and pole cell specification, but not for posterior patterning. *Genesis* **40**, 164–170 (2004).

## ONLINE METHODS

***C. elegans* strains and RNAi.** The Bristol strain N2 was used as the standard wild-type strain. Alleles used are listed by chromosome as follows: LGII: *rrf-3(pk1426), rrf-3(mg373), eri-3(tm1361)*; LGIII: *dcr-1(ok247), eri-4(mg375), rde-4(ne337)*; LGIV: *eri-1(mg366), eri-5(tm2528), drh-1(tm1329);* LGV: *rde-1(ne300). C. elegans* were cultured as previously described[33]. RNAi analysis was carried out as in ref. 34.

***C. elegans* preparations.** *C. elegans* embryonic pellets were prepared as described[13]. Samples were suspended on ice in three volumes of lysis buffer (25 mM HEPES-KOH, pH7.5, 10 mM KOAc, 2 mM $Mg(OAc)_2$, 100 mM KCl, 1% (v/v) Triton X-100 and 1 mM DTT) with a 4× concentration of Complete protease inhibitors (Roche) and homogenized in a stainless steel Dounce homogenizer for 30 to 40 strokes on ice. The resulting slurry was clarified twice at 17,000*g* for 10 min at 4 °C.

**Gel filtration analysis.** Approximately 4 mg of WT *C. elegans* embryonic extract were loaded onto an equilibrated Superose 6 gel filtration column (GE Healthcare) according to the supplier's instructions. The protein fractions were collected, precipitated with acetone, and 25 µg were loaded on a 4–15% (v/v) gel (BioRad) for western analysis.

**Multidimensional protein identification (MuDPIT).** Samples preparation and analysis were conducted as previously described[13]. For the analyses presented, previously described complex array expressing DCR-1 ∷ 8× hemagglutinin (HA), and internal ERI-1 ∷ 3× Flag fusions were used. For ERI-5 samples, affinity-purified polyclonal antibodies directed against the full-length ERI-5 (below) were used as an affinity matrix, and for RDE-4, a Flag fusion expressed from a simple array was used.

**Antibodies.** Polyclonal antibodies against RRF-3, ERI-5 and EKL-1 were raised in rabbits or mice. Anti-RRF-3 antibodies were raised against a synthetic C-terminal peptide IANNVVPNEVRDEFL, conjugated to KLH (Capralogics). Anti-ERI-5 and EKL-1 antibodies were raised to full-length *eri-5* and *ekl-1* cDNA in both rabbits (Capralogics) and mice in the case of ERI-5, and in mice only for EKL-1. Mice were handled and immunized in agreement with animal use protocol no. 5229 of the Groupe de Recherche sur le cancer McGill.

**Immunoprecipitations.** DRH-1, RDE-4, DCR-1, ERI-5, RRF-3 and EKL-1 affinity purified antibodies or antiserums were incubated with 1–5 mg of *C. elegans* embryo lysate at 4 °C for 1 h. Immune complexes were precipitated with Protein A or G Sepharose beads (GE Healthcare) or Protein A Dynabeads (Invitrogen) and washed with cold lysis buffer.

**Western blot analysis.** Proteins immobilized on a Hybond-C Extra membrane (GE Healthcare) were probed with the following antibodies: anti-DCR-1 (1:4,000), anti-RDE-1 (1:200), anti-DRH-1 (1:1,000), anti-RDE-4 (1:1,000), anti-DRH-3 (1:300), anti-ERI-5 (1:200), anti-ERI-1 (1:1,000), anti-RRF-3 (1:2,000), anti-RRF-1 (1:1,000), anti–EGO-1 (1:1,000), anti–EKL-1 (1:1,000) and anti-tubulin (1:5,000) (abcam) in PBST (137 mM NaCl, 2.7 mM KCl, 10 mM phosphate (pH 7.4), 0.1% (v/v) Tween-20) with 5% (w/v) nonfat dried milk. Rabbit and mouse TrueBlot horseradish peroxidase (HRP)-conjugated secondary antibodies (eBiosciences) were used at a ratio of 1:1,000.

**Recombinant proteins.** The cDNA for *eri-5*, *eri-3*, *ekl-1* and *dcr-1* were obtained by real-time PCR, sequenced and cloned into pCal-KC and/or pET vectors. The plasmids were transformed into ArcticExpress (DE3) (Stratagene) or BL-21 (DE3) pLysS (Promega) bacterial cells, and expression was induced with IPTG according to the supplier's instructions.

**Glutathione *S*-transferase pulldown.** Approximately 3 µg of purified DCR-1–GST fusions were incubated with glutathione-Sepharose beads (GE Healthcare) in STE buffer (10 mM Tris-HCl, pH 8.0, 150 mM NaCl, 1 mM EDTA). The bead-bound fusions were incubated 1 h with 1 µg of purified ERI-5–CBP or ERI-3–Flag recombinant proteins in bead-binding buffer (50 mM HEPES-KOH, pH 7.5, 150 mM KCl, 1 mM $Mg(OAc)_2$, 10% (v/v) glycerol, 1% (v/v) Triton X-100). GST pulldowns were washed with bead-binding buffer containing 500 mM KCl and analyzed by western blot with anti-CBP (1:1,000) (GenScript) or anti-Flag (1:2,500) (Sigma) antibodies. For the simultaneous interaction pulldown (**Fig. 2d**), 0, 0.3 and 3 µg of ERI-3–Flag were prebound to the 272–1045 fragment of DCR-1 fused to GST and bound to beads. The beads were washed, and 1 µg of ERI-5-CBP was used to assay for the second interaction, as indicated above.

**RNA preparation and northern analysis.** Total RNA from *C. elegans* embryos was prepared using the TRIZOL method (Invitrogen). Small-RNA species were enriched using the mirVana kit (Ambion). Five to ten micrograms of enriched small RNA were resolved per lane on a 15% (v/v) UREA-TBE gel. Transfer, hybridization and blot analysis were conducted as previously described[35].

**Real-time polymerase chain reaction.** For the X-cluster, small RNAs and 26G-RNA (*C40A11.10*) analyses, real-time PCR was conducted as previously described[36]. Primers used for this assay are listed in the **Supplementary Methods**.

**Small RNA cloning, deep sequencing and data analyses.** Small RNAs isolated from embryos were cloned using a 5′ ligation–dependent method as described[14], except that 5′ and 3′ adapters were ligated without pretreatment of small RNAs. This method favors the cloning of monophosphorylated, small RNAs including 26G RNAs, miRNAs and 21U-RNAs. Small RNAs isolated from adult worms were pretreated sequentially with calf-intestine phosphatase (New England Biolabs) and polynucleotide kinase (New England Biolabs), to convert the 5′ tri-phosphate of 22G RNAs to monophosphate, and then cloned as described[14]. Libraries were sequenced at the University of Massachusetts Deep Sequencing Core using an Illumina Genome Analyzer II. Data were processed and analyzed using custom PERL scripts, as described[14,20]. Data were graphed using DeltaGraph (Red Rock Software) or Prism (GraphPad).


33. Brenner, S. The genetics of *Caenorhabditis elegans*. *Genetics* **77**, 71–94 (1974).
34. Timmons, L., Court, D.L. & Fire, A. Ingestion of bacterially expressed dsRNAs can produce specific and potent genetic interference in *Caenorhabditis elegans*. *Gene* **263**, 103–112 (2001).
35. Wu, E. *et al.* Pervasive and cooperative deadenylation of 3′UTRs by embryonic microRNA families. *Mol. Cell* **40**, 558–570 (2010).
36. Raymond, C.K., Roberts, B.S., Garrett-Engele, P., Lim, L.P. & Johnson, J.M. Simple, quantitative primer-extension PCR assay for direct monitoring of microRNAs and short-interfering RNAs. *RNA* **11**, 1737–1744 (2005).





doi:10.1038/nsmb.2186

# Erratum: Tudor domain ERI-5 tethers an RNA-dependent RNA polymerase to DCR-1 to potentiate endo-RNAi

**Caroline Thivierge, Neetha Makil, Mathieu Flamand, Jessica J Vasale, Craig C Mello, James Wohlschlegel, Darryl Conte Jr & Thomas F Duchaine**

*Nat. Struct. Mol. Biol.* **19, 90–97 (2012); published online 18 December 2011; corrected after print 9 January 2012**

In the version of this article initially published, information in Table 1 was inaccurate. "Newly described" should have been "novel" and "Argonaute protein domain" should have read "Argonaute protein." The errors have been corrected in the HTML and PDF versions of the article.